White Rose
university consortium
Universities of Leeds, Sheffield & York

eprints@whiterose.ac.uk
https://eprints.whiterose.ac.uk/

Temperature-programmed reduction of nickel steam reforming catalyst with glucose

Feng Cheng [a],[*], Valerie Dupont [a], Martyn V. Twigg [b]

[a] *Energy Research Institute, School of Chemical and Process Engineering, The University of Leeds, Leeds, LS2 9JT, UK*
[b] *Twigg Scientific & Technical Ltd, Caxton, Cambridge, CB23 3PQ, UK*

ABSTRACT

Temperature-programmed reduction (TPR) of a NiO/α-Al$_2$O$_3$ steam reforming catalyst with glucose under a N$_2$ flow was investigated using TGA-FTIR technique. A series of catalyst samples obtained at different temperatures during the TPR were characterised by XRD, CHN elemental analysis, SEM-EDX and TPO. Results showed that the whole TPR covering from room temperature to 900 °C consisted of two reactive processes. They were glucose pyrolysis producing carbonaceous materials (char), and NiO reduction by the char resulting in CO$_2$ as a main product. When the initial mass ratio of glucose to the catalyst was 1:10, the catalyst could be completely reduced without carbon remaining. Moreover, two mass loss peaks were observed at around 440 °C and 670 °C, respectively, during the reduction. Based on the experiments of char characterisation, H$_2$ TPR and excess glucose TPR, a two-stage reduction mechanism was proposed. The first reduction stage was attributed to a solid reaction between NiO and char. The second stage was assigned to NiO being reduced by the CO produced by char gasification with CO$_2$. Their apparent activation energies were 197 ± 19 kJ/mol and 316 ± 17 kJ/mol, respectively, estimated using the Kissinger method.

© 2016 Published by Elsevier B.V.

1. Introduction

Chemical looping reforming (CLR) is a novel reforming technology for syngas production from hydrocarbons with low heat demand [1–5]. A typical CLR process is performed by circulating oxygen carrier (normally supported metal oxide) between two reactors. In a fuel reactor, the oxygen carrier is first reduced by fuel, and then catalyses steam reforming of fuel [6]. In an air reactor, the reduced oxygen carrier is re-oxidized and then sent back to the fuel reactor for a new cycle. The heat required for the steam reforming is supplied by the internal combustion. A key issue for CLR technology is the selection of suitable oxygen carriers. Supported NiO has been suggested as a promising oxygen carrier due to its high reduction reactivity and adequate catalytic activity on steam reforming [6–8].

In fact, alumina supported NiO (NiO/α-Al$_2$O$_3$) is a common catalyst for industrial steam reforming process [9]. It has also been selected as a model steam reforming catalyst in some research [10,11]. Similar to other transition metal catalysts, the NiO catalyst requires reduction to give active phase (i.e. metallic Ni) prior

to their use [12]. In industry, the catalyst reduction is usually conducted with either hydrogen-containing gases or natural gas-steam mixtures. Reduction conditions are important as they have influences on subsequent catalytic activity [10]. For instance, high temperatures and rapid reduction may result in lower Ni dispersions and less activity, the introduction of carbon or sulphur may accelerate catalyst deactivation [13,14]. Therefore, reduction mechanisms and possible affecting factors have been extensively investigated using hydrogen or light hydrocarbons as reducing agents [15–22].

Richardson et al. [10,11,16] carried out a series of studies on H$_2$ reduction of NiO/α-Al$_2$O$_3$ catalysts. A reduction mechanism was proposed as follows. (1) Hydrogen is dissociated, first on NiO and then rapidly on the surface of Ni clusters as they become available. (2) Hydrogen atoms rupture Ni—O bonds, producing Ni^0 atoms and H$_2$O molecules. This process is retarded or accelerated by foreign cations in NiO lattice or on vicinal surface. (3) Nickel atoms diffuse across the support surface away from reduction centres. Water retained on the surface retards nucleation by limiting the diffusion. (4) Nickel atoms nucleate into metallic clusters, after an induction period if the overall reduction rate is low (e.g. at low temperatures). (5) Nickel clusters grow into crystallites. In addition to chemical reaction, nucleation and mass transfer, the fate and activity of radicals formed by the dissociation of reductant molecules

* Corresponding author.
E-mail addresses: fengcheng@njust.edu.cn (F. Cheng), V.Dupont@leeds.ac.uk (V. Dupont).

also play a role in determining reduction kinetics, as suggested by Syed-Hassan et al. [18,23].

The conventional fuel for syngas generation by steam reforming or CLR is natural gas. There is a growing interest in exploiting biomass as substitute of fossil fuel to produce fuels and chemicals. Some bio-liquids such as bio-diesel and bio-ethanol could be utilized as transport fuels after a simple pre-treatment. In contrast, bio-oil must be upgraded by complex chemical processes (e.g. hydrodeoxygenation, zeolite upgrading [24]) if it is to be used in vehicles, which increases energetic and economic costs. This is determined by the properties of bio-oil that include high oxygen content, complex composition, low heating value, high viscosity, incomplete volatility, and chemical instability. Alternatively, bio-oil can be converted into syngas by steam reforming [25,26]. The conversion of bio-liquids to syngas is a promising route to utilize biomass resources as syngas has a wide application (the production of ammonia, methanol, alkanes and hydrogen), although the storage of syngas is not as easy as that for liquid fuels. Syngas production by bio-oil steam reforming followed by water gas shift has been considered as a promising way for sustainable H_2 production, which is of importance to accomplish 'hydrogen economy' in future.

Some bio-liquids (e.g. sunflower oil [2], waste cooking oil [27,28], scrap tyre oil [29], and bio-oil [30]) have been tested in a CLR process. Feasibility of bio-oil CLR was proved but bottlenecks still existed. For scrap tyre pyrolysis oil in which a considerable amount of sulphur was present [29], the H_2 yield decreased as the cycle number increased. Analysis of the reacted catalyst indicated this was most likely due to catalyst deactivation by carbon deposition and sulphur poisoning. Catalyst deactivation upon cycling was also observed during the CLR of biomass pyrolysis oil as indicated by the drop in fuel conversion [30]. The reduction rate of catalyst also decreased with cycling. Solutions to these problems include preparing catalysts more tolerant to carbon deposition, pre-treating feedstock to remove sulphur, and investigating the mechanism of catalyst reduction with bio-feedstock.

As a typical bio-feedstock for CLR, bio-oil is obtained by fast pyrolysis of biomass and comprised of numerous hydrocarbons. Most of bio-oil components have a tendency to decompose at operating temperatures (600–900 °C). Both types of pyrolysis products (volatiles and char) are potential reductant for oxygen carriers. Therefore, multiple reaction channels exist simultaneously during CLR, making research on reduction mechanism difficult.

Rather than evaluating the global reduction process during CLR, the objective of this study is to reveal the reactivity between a NiO catalyst and char from glucose pyrolysis, which is part of the complex reaction network. Glucose was selected as a model compound of biomass as it is the basic building block of cellulose and one of bio-oil components [25,26]. A slow temperature-programmed rise and a continuous flow of inert gas were employed in this study. Such a condition decoupled glucose pyrolysis and catalyst reduction, enabling the reduction to be studied separately. Reduction characteristics and mechanism were discussed. The work presented here is part of a series on the reduction of a NiO catalyst with various bio-compounds and has been covered in the thesis of the first author [8]. Such a study has an implication both for exploiting biomass resources via chemical looping technology and for gaining an insight into solid reduction mechanism.

2. Experimental

2.1. Sample preparation

The catalyst used in this study was 18 wt % NiO/α-Al$_2$O$_3$ provided by Johnson Matthey Plc. It was received as pellets and was

broken into particles with a size of 0.85–2 mm prior to use. As Fig. 1 displays, the fresh catalyst particles showed uniform grey green. After being reduced by H_2, they turned to uniform black. Presumably, NiO was distributed throughout the pellet rather than like an eggshell. Glucose ($C_6H_{12}O_6$) was purchased from Fisher Scientific. The catalyst particles (2.0 g) were impregnated with a glucose aqueous solution (20 mL, 10 g/L) overnight at room temperature without stirring. Then the particles were dried at 80 °C in an oven for about 12 h and hereafter denoted as 'catalyst-G'. For control experiments, blank α-Al$_2$O$_3$ pellets (provided by TST Ltd.) were treated using the same procedure as the catalyst. The α-Al$_2$O$_3$ particles impregnated with glucose were referred to as 'Al$_2$O$_3$-G'. The NiO/α-Al$_2$O$_3$ particles without impregnation were referred to as 'fresh catalyst'.

2.2. Temperature-programmed reduction (TPR)

(1) For process analysis, the TPR of catalyst-G was performed on a TGA-FTIR instrument. A thermal gravity analyser (TGA, Stanton Redcroft TGH1000) and a Fourier transform infrared spectroscope (FTIR, Thermo Scientific Nicolet iS10) were integrated via a Nicolet transfer line. 200 mg of samples were placed in a platinum crucible and heated from ambient temperature to 900 °C at 5 °C/min under a N_2 flow of 50 mL/min. The Nicolet's OMNIC software was used to analyse FTIR spectra and create chemigrams (species evolution profile against temperature). Wavenumber ranges set for creating the chemigram of a specific compound were listed in SD1 (Supplementary Document 1). (2) For kinetics analysis, a series of TPR experiments were carried out by the TGA instrument alone. The heating rate was maintained at 5 °C/min for the process of glucose pyrolysis but changed to different values (3, 7, 10, 15 °C/min) when it came to the process of NiO reduction. (3) The H_2 TPR experiment was also performed on the TGA instrument. 20 mg of fresh catalyst were heated from ambient to 150 °C at 20 °C/min under a N_2 flow and then was kept at this temperature for 3 h to remove adsorbed moisture and air. After that, the sample was heated to 900 °C at 5 °C/min under a H_2 flow (5% H_2 in N_2, 50 mL/min) followed by naturally cooling down under a N_2 flow. (4) The excess glucose TPR experiment was conducted in the same procedure as that for catalyst-G, except that the initial mass ratio of glucose to the catalyst was 1:1.4 in contrast to the 1:10 for catalyst-G.

2.3. Sample characterisation

A series of samples were obtained at different temperatures during the TPR of catalyst-G. They were denoted as 'catalyst-G-T', where 'T' stands for the end temperature (420, 530, 670, 770 or 900 °C). They were crushed to fine powder for XRD tests, CHN elemental analysis and TPO tests but were kept as particles in SEM-EDX tests.

2.3.1. XRD and Rietveld refinement

X-ray diffraction (XRD) tests of these samples were conducted using a PANalytical X'pert MPD instrument with Cu Kα radiation. The scanning of X-ray ranged from 20° to 80° (2θ) with an increment of 0.0332°/step and a speed of 0.7 s/step. To determine crystallite sizes of Ni and NiO, Rietveld refinement of the XRD data [31] was performed using X'Pert HighScore Plus software.

2.3.2. CHN elemental analysis

The carbon and hydrogen content of these samples was determined by a CHN elemental analyser (Flash EA2000 by CE Instruments Ltd.). Around 15 mg of powder samples was put into a tin capsule. Then the tin capsule was folded properly to remove any trapped air before it was fed to the analyser. Duplicate determina-

Fig. 1. Photos of catalyst pellet, fresh catalyst particles and reduced catalyst particles.

tion was made and a good repeatability was achieved. The mean values were reported in this paper.

2.3.3. Temperature-programmed oxidation

Temperature-programmed oxidation (TPO) was carried out on the TGA-FTIR instrument. About 150 mg of powder samples was heated from ambient temperature to 900 °C at 5 °C/min in air flow (50 mL/min). The mass loss was monitored by TGA and meanwhile the evolved gases were online analysed by FTIR.

2.3.4. SEM-EDX

A field-emission scanning electron microscope (SEM, LEO 1530) coupled with energy dispersive X-ray spectrometer (EDX, Oxford Instruments AztecEnergy) was employed to show morphology and element distribution of the fresh and reacted catalysts. The particle samples were mounted on a sticky pad of a SEM stem and then coated with a platinum layer of 10 nm prior to SEM-EDX tests.

3. Results and discussion

3.1. TPR process analysis

TGA-FTIR results for catalyst-G under N_2 at a heating rate of 5 °C/min are presented in Fig. 2, and compared with those for Al_2O_3-G. As indicated by the differential thermal gravity (DTG) curves (Fig. 2b), both samples underwent several mass losses. CO_2, H_2O and formic acid were identified in the volatile product (see SD1), and their evolution profiles against temperature are displayed in Fig. 2c–e.

Up to 420 °C (process A in Fig. 2), both catalyst-G and Al_2O_3-G exhibited a similar mass change pattern that was an obvious mass loss over 150–240 °C followed by a less pronounced mass loss. These mass losses corresponded to the emission of CO_2, H_2O and formic acid. For each volatile product, its evolution profile from catalyst-G was almost the same as that from Al_2O_3-G. The good agreement of catalyst-G with Al_2O_3-G in terms of mass loss and product evolution suggested NiO took no part in related reactions. Since α-Al_2O_3 was known as inert refractory material, glucose pyrolysis [32] might be the only global reaction in this process.

From 420 °C to 900 °C (process B in Fig. 2), two additional mass losses around 440 °C and 670 °C were observed on catalyst-G but not on Al_2O_3-G. These two mass losses were mainly attributable to CO_2 generation (Fig. 2c). Some water vapour (to a much lower extent) was also evolved as shown in Fig. 2d, contributing to the mass losses. Until now, it is reasonable to presume that NiO reduction took place in process B with CO_2 as the main product. If using CH_nO_k to represent the actual reductant (i.e. the char formed by
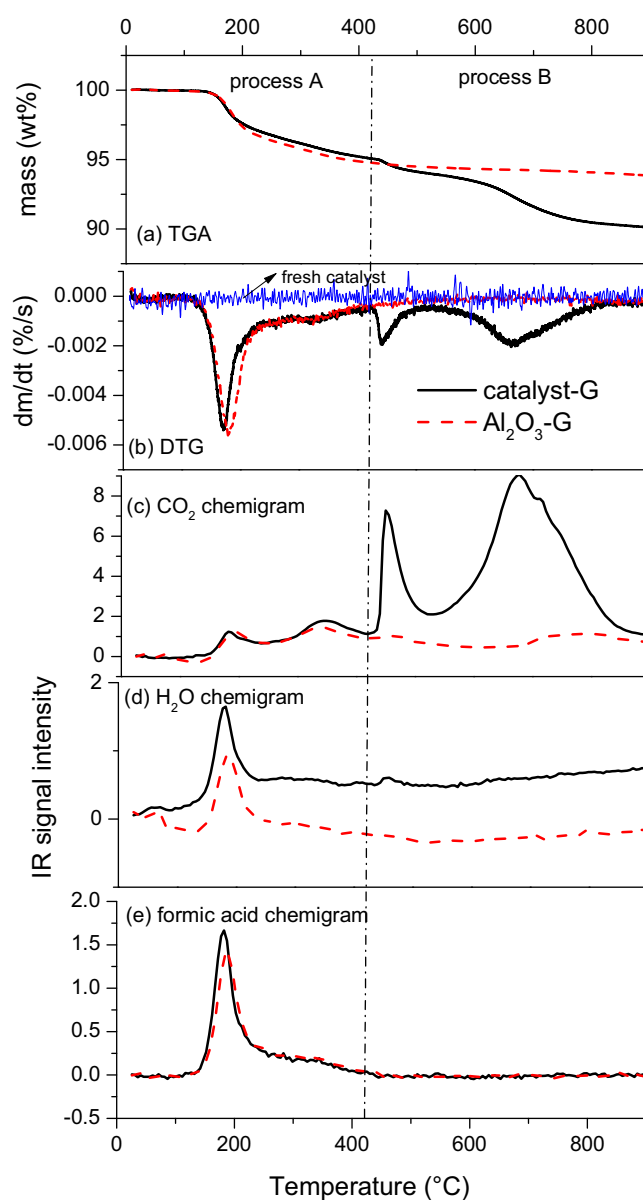

Fig. 2. TGA-FTIR results of catalyst-G (solid line) and Al_2O_3-G (dashed line) under N_2 at the heating rate of 5 °C/min: (a) TGA curve, (b) DTG curve, (c) CO_2 evolution profile, (d) H_2O evolution profile and (e) formic acid evolution profile. DTG of fresh catalyst is also shown in (b).
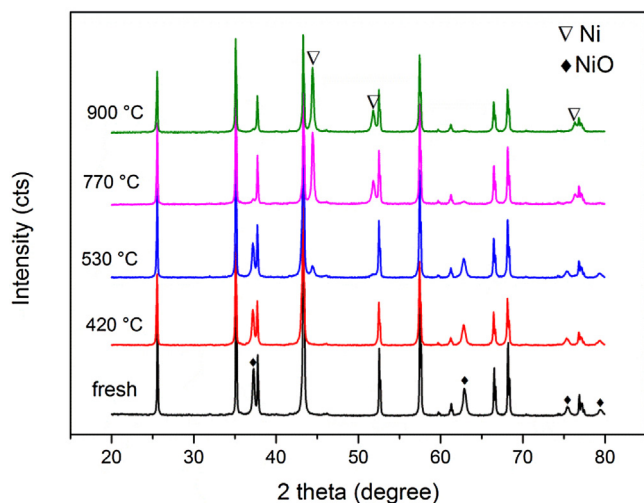
Fig. 3. XRD patterns of catalyst-G-T samples and fresh catalyst (T=420, 530, 770, 900 °C, unmarked peaks are attributed to α-Al_2O_3).

Fig. 4. Carbon and hydrogen content of catalyst-G-T samples (T=420, 530, 670, 770 and 900 °C), catalyst-G and fresh catalyst.

glucose pyrolysis), the global reduction reaction can be postulated as below:

$$CH_nO_k + (2 + 0.5n-k)NiO \rightarrow CO_2 + 0.5nH_2O + (2 + 0.5n-k)Ni$$

Sharma et al. [33] suggested that both CO_2 and CO were primary products of NiO reduction with graphite in the temperature range of 900–1000 °C. However, CO was not detected in this work probably due to the relatively low reaction temperature (below 900 °C). This explanation was supported by a thermodynamic analysis (see SD2) that indicated the generation of CO was more thermodynamically favourable than the generation of CO_2 at elevated temperatures during NiO reduction with carbon.

In order to further verify the occurrence of NiO reduction, XRD analysis of the catalyst-G-T samples obtained at different TPR end temperatures was conducted. As Fig. 3 shows, the characteristic peaks of metallic Ni were not observed at 420 °C but clearly appeared at 530 °C. This result, combined with the TGA-FTIR result in Fig. 2, indicated the onset temperature of NiO reduction was 420 °C. As the temperature rose, the intensity of Ni peaks increased while the intensity of NiO peaks decreased. When the temperature was raised to 900 °C, the NiO peaks entirely disappeared, suggesting the reduction was completed.

3.2. Characteristics of char and reacted catalyst

As discussed in Section 3.1, the char from glucose pyrolysis acted as actual reductant for the catalyst reduction. To better understand this reaction, properties of the char, which usually include its amount, its composition (H/C ratio), its homogeneity, and its location on the catalyst, were discussed in this section. In addition, the change of Ni crystallite size during TPR was also analysed since the performance of supported metal catalyst for reforming reactions is affected by the metal crystallite size.

3.2.1. Carbon and hydrogen content of char (CHN results)

Carbon and hydrogen contents of the catalyst-G-T samples (T = 420, 530, 670, 770 and 900 °C) are presented in Fig. 4. The far left points in Fig. 4 represent the carbon and hydrogen contents of catalyst-G (before thermal treatment). The original carbon and hydrogen contents of the fresh catalyst are also shown using horizontal lines, below which the element content could be considered negligible.

As seen in Fig. 4, a carbon loading of 2.69 wt% to the catalyst was achieved by impregnation. As the temperature increased, the

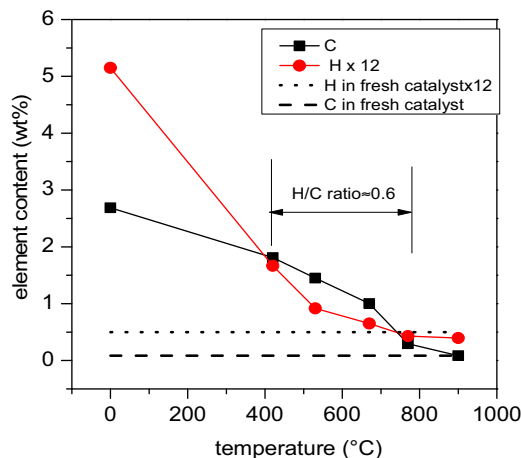amount of carbon on the catalyst decreased gradually until it was depleted at 900 °C. At the end of glucose pyrolysis and the beginning of NiO reduction (T = 420 °C), the carbon content was 1.72 wt%. This was the actual amount of carbon available for NiO reduction. It was collectively determined by the amount of glucose input, the charring property of glucose, the pyrolysis condition employed and some other factors. To quantify the charring property of a carbon source, the term 'carbon deposition efficiency' (CDE), defined as the mass ratio of the carbon deposited via pyrolysis to the carbon initially present in the feedstock, is introduced. The CDE of catalyst-G was 64%, higher than that for pure glucose (50% obtained by a pyrolysis experiment of pure glucose). The enhanced charring ability could be ascribed to the presence of solid support. Besides, we also found that the CDE varied with the type of feedstock. Citric acid ($C_6H_8O_7$), another common compound existing in plants, was treated using the same impregnation procedure and then the same TGA condition as glucose. CHN elemental analysis showed that the CDE of the catalyst-citric acid system was only 30%, much lower than that of catalyst-G. As a result of deficient reductant, the conversion of NiO to Ni was only 68% although the initial amount of carbon source was the same as that for catalyst-G. Compared with citric acid, glucose is more suitable as a carbon source since a high CDE is favourable for achieving a complete reduction in the absence of other reducing agents.

In order to calculate the molar ratio of hydrogen to carbon (H/C ratio), the weight percentage of hydrogen was multiplied by 12 (i.e. the molar mass of carbon) and then compared with the weight percentage of carbon, as shown in Fig. 4. The initial H/C ratio was 1.92, in good agreement with the expected value of 2.00 according to the molecular formula of glucose. A dramatic decrease in the H/C ratio occurred during the process of glucose pyrolysis. After that, the H/C ratio remained constant at around 0.6 throughout the reduction process. If oxygen in the char was not taken into consideration, the char could be expressed as $CH_{0.6}$, approaching to the coke deposited on bi-functional catalysts during steam reforming of naphtha with a H/C ratio varying from 0.5 to 1 [34].

Based on the carbon content and the NiO content of the catalyst-G-420, the molar ratio of $CH_{0.6}$ to NiO was calculated to be 0.61, larger than the stoichiometric ratio of 0.43 (= 1/2.3) for reaction R1 shown below. Therefore, the amount of reductant char was theoretically sufficient for complete reduction, a feature verified by the lack of NiO peaks in the XRD pattern beyond 770 °C (Fig. 3). Correspondingly, measurable excess reductant was expected to remain in the catalyt-G-900 sample. Nonetheless, little carbon or hydro-
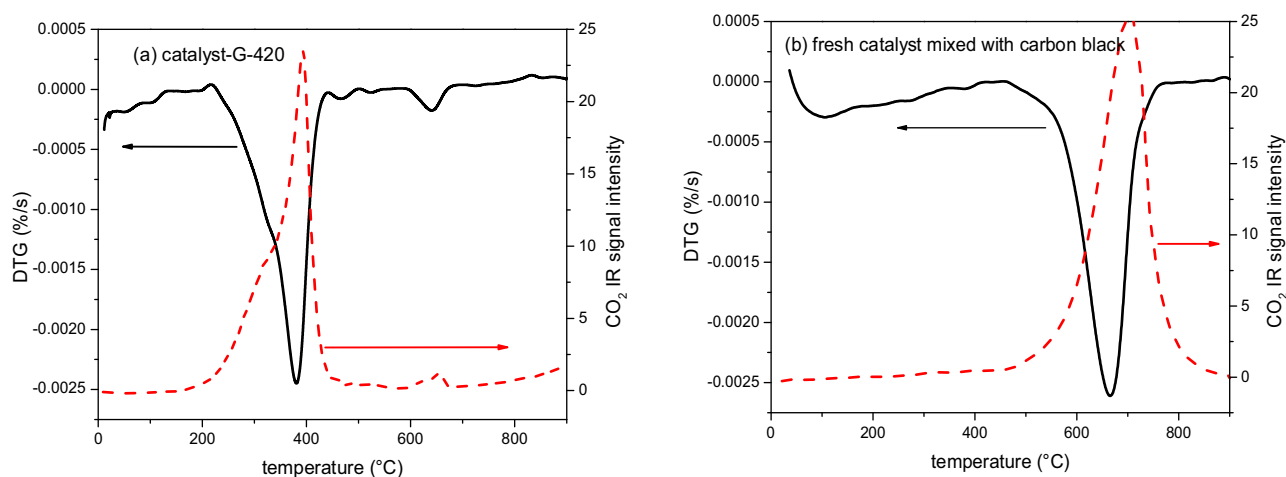
Fig. 5. DTG curves and CO_2 chemigrams in the TPO experiment of (a) catalyst-G-420, (b) the mixture of fresh catalyst and carbon black (the mass ratio is 10:1) under an air flow of 50 mL/min at a heating rate of 5 °C/min.
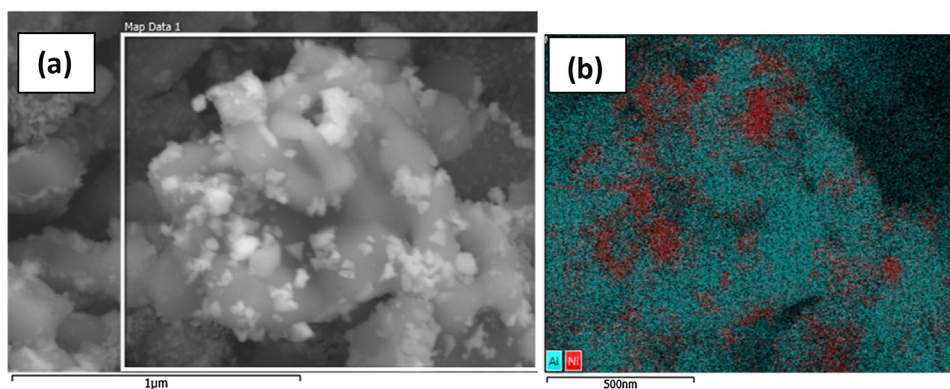

Fig. 6. (a) SEM image and (b) EDX mapping of fresh NiO/α-Al$_2$O$_3$ catalyst (red colour for Ni element and blue for Al element). (For interpretation of the references to colour in this figure legend, the reader is referred to the web version of this article.)

Fig. 7. (a) SEM image and (b) EDX mapping of the catalyst-G-420 sample (red for Ni element, pink for carbon element and blue for Al element). (For interpretation of the references to colour in this figure legend, the reader is referred to the web version of this article.)
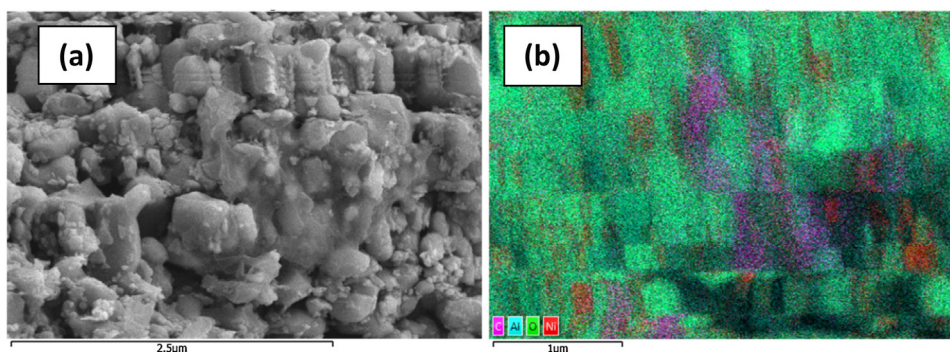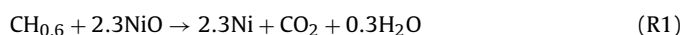
gen was detected, indicating the carbonaceous material had some volatility/reactivity besides that of the reduction mechanism.

$$CH_{0.6} + 2.3NiO \rightarrow 2.3Ni + CO_2 + 0.3H_2O \quad \text{(R1)}$$

3.2.2. The homogeneity of char (TPO results)

TPO results of the catalyst-G-420 and the catalyst/carbon black mixture are shown in Fig. 5. A main mass loss peak accompanied by a CO_2 evolution peak was observed at around 385 °C for the catalyst-G-420 (Fig. 5a). Another mass loss peak appeared at around 650 °C but its intensity was quite small. Hence, it is reasonable to believe that the char was almost homogenous [35]. Compared with carbon black (Fig. 5b), the char showed a much lower oxidation temperature (385 °C vs. 650 °C), probably because of its higher H content. The H/C ratio of the glucose char is as high as 0.6 whereas the carbon black contains more than 97% carbon.

3.2.3. Distribution of char over NiO/α-Al$_2$O$_3$ (SEM-EDX results)

Fig. 6 shows the SEM image of fresh catalyst and corresponding EDX mapping. As seen in Fig. 6, the NiO exists in the form of particles that are scattered over α-Al$_2$O$_3$ support. These NiO particles show a wide size distribution from tens to hundreds of nanometres. The
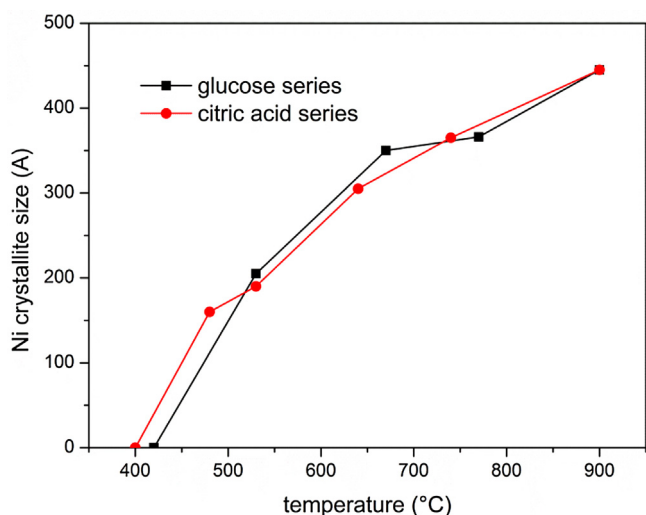
Fig. 8. The dependence of Ni crystallite size on temperature during the TPR of catalyst-G and catalyst-citric acid.

mean size of NiO crystallites is about 40 nm, derived by the Rietveld refinement of XRD data. Thus, larger NiO particles are likely to be the aggregation of NiO crystallites. While the morphological feature of the catalyst could be very complex, it is clear that a fraction of the α-Al$_2$O$_3$ surface is uncovered. To show the morphology of the char, the catalyst-G-420 sample was selected for SEM-EDX characterisation as it had the largest amount of char. As Fig. 7 displays, the char exists as a layer covering the catalyst unevenly and some NiO sites are bare.

3.2.4. Ni crystallite size

The change of Ni crystallite size with temperature during the TPR process is shown in Fig. 8. The Ni crystallite size increased with the temperature and reached the maximum (44 nm) at the end of TPR (T = 900 °C). To check the influence of reductant on Ni crystallite size, citric acid was used in the same TPR process instead of glucose. CHN elemental analysis indicated that the H/C ratio of citric acid char was around 1, different from that of glucose char. When the citric acid char acted as reductant, the Ni crystallite size approximated to that for glucose char. This result suggested that the Ni crystallite size was mainly affected by the temperature. The type of reductant had little effect.

3.3. Reduction mechanism

As Fig. 2b-c show, two reduction peaks were observed during the TPR of catalyst-G. The occurrence of multiple reduction stages has been reported in the literature [36,37] and usually attributed to (1) the existence of different NiO species (free NiO, and the NiO strongly combined with Al$_2$O$_3$, i.e. NiAl$_2$O$_4$) and (2) the heterogeneity of reductant. These two possibilities, however, were excluded in this study. First, there was no evidence for NiAl$_2$O$_4$ formation as only the reduction peak of NiO was observed in the H$_2$ TPR profile (Fig. 9). Besides, there was no indication of any phase other than Ni, NiO and α-Al$_2$O$_3$ in the XRD profiles (Fig. 3). Second, it was not reasonable to attribute the two reduction peaks to the existence of two types of carbonaceous materials in the char because only one main mass loss peak was shown in the TPO profile of catalyst-G-420 (Fig. 5a).

In the work of El-Guindy and Davenport on ilmenite reduction with graphite [38], two reduction stages were also observed, which was explained as follows. The first reduction stage was assigned to the solid-solid reaction. The second reduction stage occurring at a higher temperature was attributed to the reduction with CO that
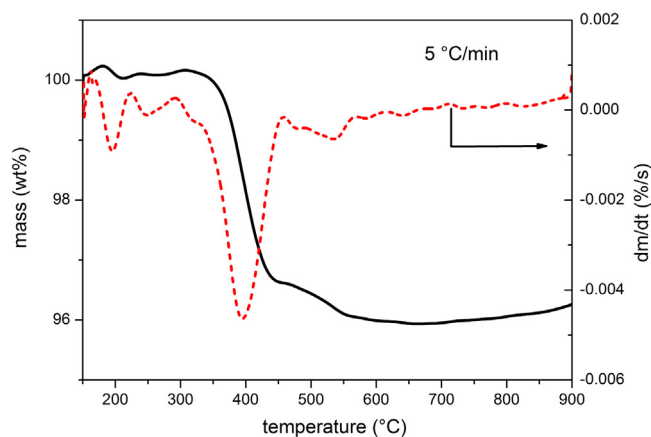

Fig. 9. TGA and DTG curves in the H$_2$ TPR experiment of the NiO/α-Al$_2$O$_3$ catalyst.
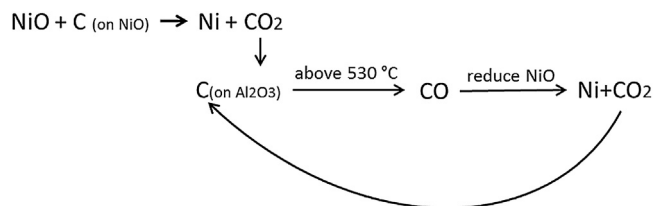

Fig. 10. Schematic of the NiO/α-Al$_2$O$_3$ catalyst reduction with the char deposited on it.

was regenerated via reaction R3. Pan et al. [39] suggested the direct reduction of CuO by coal char could take place at temperatures as low as 500 °C. As the temperature rose, the reactivity of char gasification (R3) was increased and its product CO became the main reducing agent for CuO reduction.

$$2NiO + C \rightarrow 2Ni + CO_2 \qquad (R2)$$

$$C + CO_2 \leftrightarrow 2CO \qquad (R3)$$

$$NiO + CO \rightarrow Ni + CO_2 \qquad (R4)$$

Similarly, a two-stage reduction mechanism was proposed in this study to explain the two reduction peaks observed during TPR. As illustrated in Fig. 10, the NiO first reacted with the char deposited on NiO sites and produced CO$_2$ (R2), which accounted for the first reduction peak over 420–530 °C shown in Fig. 2b-c. The reduction was accelerated by the rising temperature but slowed down by the decreased amount of the char. As a result of the competition between these two factors, the first reduction peak was formed with the maximum rate at 440 °C. When the temperature was increased above 530 °C, the gasification of char with CO$_2$ (R3) was initiated. Thermodynamic calculation (see SD3) also indicates that the generation of CO via R3 does not occur until 500 °C. Through CO$_2$ gasification, the char deposited on the Al$_2$O$_3$ surface was converted to CO, which acted as a reducing agent for the second reduction stage (R4). The CO$_2$ produced via reaction (R4) would react with the char in return to give more CO. Therefore, CO and CO$_2$ were regenerated cyclically as illustrated in Fig. 10. Because of the continuous supply of CO, the reduction of NiO particles that were not covered by char became possible. Such a reduction process could be understood as the reductant char was transported from Al$_2$O$_3$ sites to NiO sites with CO$_2$ as intermediate mobile carrier.

To test this two-stage reduction mechanism, an excess glucose TPR experiment was conducted (see Section 2.2). The mass ratio of glucose to the catalyst was set at 1:1.4 so that the amount of glucose was considerably excessive for complete reduction of the catalyst. The TPR result is shown in Fig. 11 and compared with that for catalyst-G. When an excess of glucose was used, the catalyst was
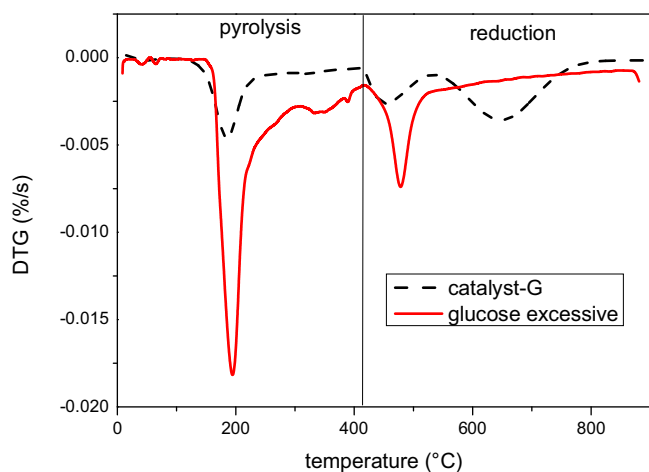
Fig. 11. TPR profiles of the NiO/α-Al$_2$O$_3$ catalyst covered by excessive glucose (the mass ratio of glucose to the catalyst is 1:1.4) and the catalyst-G under a N$_2$ flow at a heating rate of 10 °C/min.
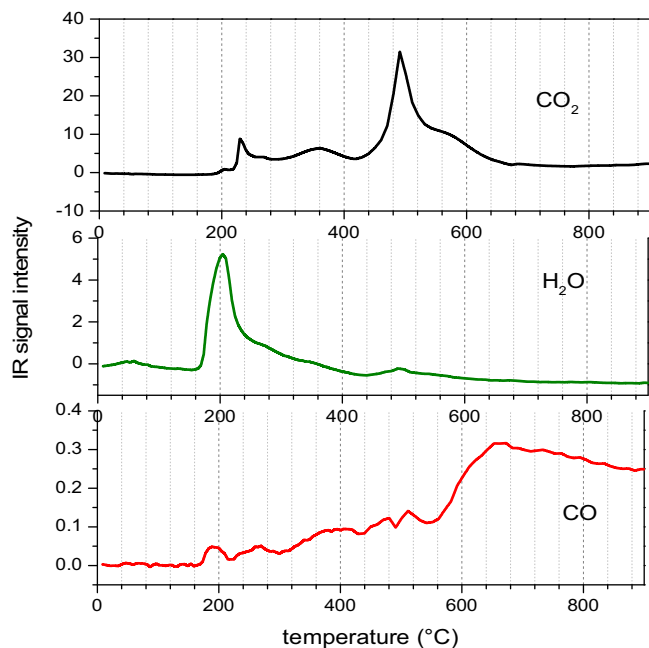

Fig. 12. Evolution profiles of CO$_2$, H$_2$O and CO with respect to temperature during the TPR of the NiO/α-Al$_2$O$_3$ catalyst covered by an excess of glucose.

Fig. 13. DTG curves of catalyst-G under N$_2$ with a constant heating rate (5 °C/min) for glucose pyrolysis and different heating rates (3, 7, 10 and 15 °C/min) for the reduction process.

Fig. 14. Kissinger plots for the two reduction peaks observed in the TPR of catalyst-G.

expected to be entirely covered by the char from glucose pyrolysis. Thus all the NiO particles could be directly reduced by the char in contact with them. This hypothesis was supported by the experimental evidence that only one reduction peak over 420–530 °C was observed during the excess glucose TPR. According to the reduction mechanism, the CO produced via char gasification was expected to be detected at temperatures above 530 °C since the NiO reduction that would consume CO had been completed. Such an inference was validated by the evolution of CO following reduction, as displayed in Fig. 12.

3.4. Apparent activation energy

To study the kinetics of the catalyst reduction, a series of TPR runs were done by using different heating rates for the reduction process (above 420 °C). Corresponding DTG curves are presented in Fig. 13, from which two sets of reduction peaks are clearly identifie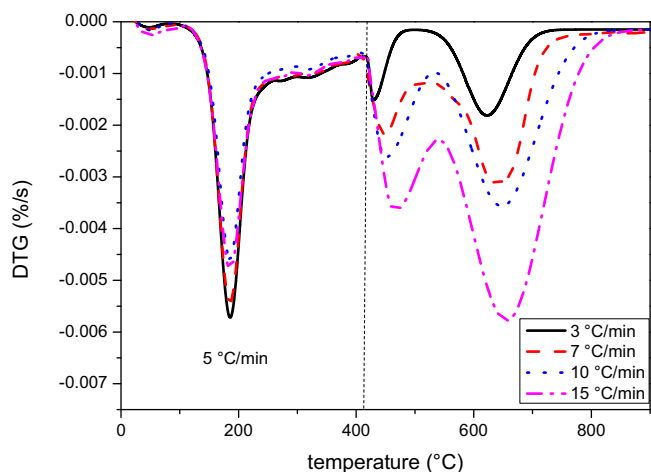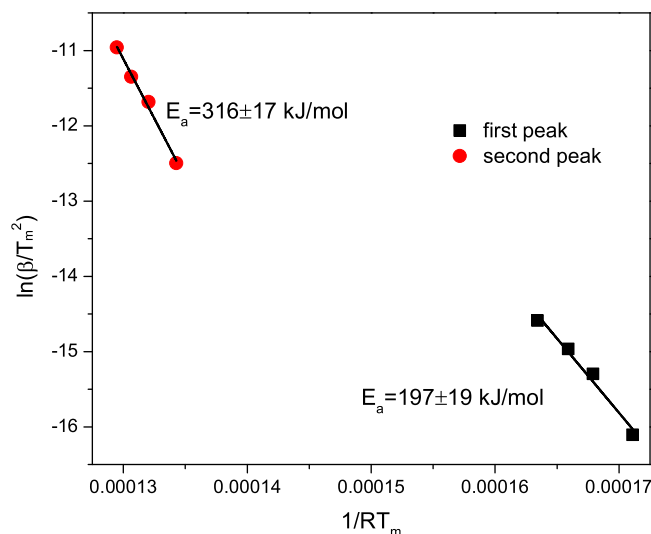d around 440 °C and 670 °C, respectively. For each reduction peak, the peak maximum (apex) corresponds to the largest mass loss rate and thus the maximum reduction rate. The variation of the temperature for the maximum reduction rate (T_m) with heating rate (β) could be expressed by Eq. (1) where E_a is the apparent activation energy, R the gas constant and A the pre-exponential factor of Arrhenius equation [40]. According to Eq. (1), the E_a and A could be derived from the slope and the intercept of Kissinger plot, which is $\ln(\beta/T_m^2)$ versus ($1/RT_m$). This procedure is known as the Kissinger method [40].

$$\ln\left(\frac{\beta}{T_m^2}\right) = -\frac{E_a}{RT_m} + \ln\left(\frac{AR}{E_a}\right) \tag{1}$$

Kissinger plots for the two reduction stages are presented in Fig. 14, yielding an activation energy of 197 ± 19 kJ/mol and 316 ± 17 kJ/mol, respectively. According to previous studies, the E_a for NiO reduction with H$_2$ was around 90 kJ/mol [15,16,40–42] and 114 kJ/mol with CH$_4$ [43]. The E_a obtained in this study for NiO reduction by char (R2) was higher, probably due to the nature of solid-solid reaction. But compared to the reduction of bulk NiO with graphite (314 kJ/mol [33]), the E_a for the reduction of the NiO catalyst with char was much lower (197 kJ/mol). Suggested by our experiment (SD4) and the literature [11,16], the reduction of sup-

ported NiO should be more difficult than that of bulk NiO when the reductants used are the same. Therefore, the lower E_a value in this study could not be ascribed to the presence of the α-Al_2O_3 support. A possible explanation is that the char from glucose pyrolysis is more active than graphite due to its high hydrogen content. A high activity of glucose char had been suggested by its considerably low oxidation temperature compared with carbon black (see Fig. 5). For the second reduction stage, the E_a was as high as 316 ± 17 kJ/mol although gaseous reductant CO was involved. It seemed that the generation of CO by char gasification which usually showed a high E_a value (240 kJ/mol for coal char reported in [44]) was the rate controlling step.

4. Conclusions

There is a growing interest in converting biomass to syngas by chemical looping reforming (CLR) technology. The reduction of an oxygen carrier by bio-feedstock is an important part of a CLR process. This paper investigated the reaction between a NiO/α-Al_2O_3 catalyst and glucose in a batch pyrolysis mode using TGA-FTIR technique. A mixture of glucose and the catalyst was prepared by impregnation and then submitted to a slow temperature-programmed rise (5 °C/min) under a N_2 flow. Such a condition enabled the separation of glucose pyrolysis and catalyst reduction. Through pyrolysis, about 64% of the carbon in glucose molecules was converted to char which later acted as reductant. The char was almost homogeneous and showed a H/C ratio of 0.6. It was unevenly distributed on the catalyst surface with some NiO uncovered. The catalyst reduction started at 420 °C, mainly producing CO_2. A complete reduction without carbon remaining was achieved when the mass ratio of glucose to the catalyst was 1:10 under our experimental condition. The crystallite size of product Ni increased with temperature during the TPR and reached 44 nm at the end of TPR (900 °C). A two-stage reduction mechanism was proposed to explain the two reduction peaks observed during the TPR. NiO first reacted with the char deposited on NiO sites. The reaction was accelerated by the increasing temperature but slowed down by the decrease in the amount of char. As a result, a reduction peak centred at 440 °C was observed during TPR. When the temperature was raised to above 530 °C, the gasification of char by CO_2 was initiated and produced CO, which acted as reductant for the following reduction centred at 670 °C. The apparent activation energy for these two reduction stages was 197 ± 19 kJ/mol and 316 ± 17 kJ/mol, respectively. Such a mechanism made possible the transport of char from α-Al_2O_3 sites to NiO sites and the reduction of the NiO uncovered by char. Future work on the reduction of NiO catalyst with other biomass derivatives such as citric acid is in progress.

References

[1] J. Adanez, A. Abad, F. Garcia-Labiano, P. Gayan, L.F. de Diego, Prog. Energy Combust. Sci. 38 (2012) 215–282.
[2] V. Dupont, A.B. Ross, I. Hanley, M.V. Twigg, Int. J. Hydrogen Energy 32 (2007) 67–79.
[3] M. Ryden, A. Lyngfelt, T. Mattisson, Fuel 85 (2006) 1631–1641.
[4] M.M. Hossain, H.I. de Lasa, Chem. Eng. Sci. 63 (2008) 4433–4451.
[5] M. Johansson, T. Mattisson, A. Lyngfelt, A. Abad, Fuel 87 (2008) 988–1001.
[6] A. Cabello, P. Gayán, F. García-Labiano, L.F. de Diego, A. Abad, M.T. Izquierdo, J. Adánez, Appl. Catal. B: Environ. 147 (2014) 980–987.
[7] Q. Zafar, T. Mattisson, B. Gevert, Ind. Eng. Chem. Res. 44 (2005) 3485–3496.
[8] F. Cheng, Bio-compounds as Reducing Agents of Reforming Catalyst and Their Subsequent Steam Reforming Performance Thesis (Ph.D.), University of Leeds, 2014 (URI:) http://etheses.whiterose.ac.uk/id/eprint/7715.
[9] L.F. de Diego, M. Ortiz, J. Adanez, F. Garcia-Labiano, A. Abad, P. Gayan, Chem. Eng. J. 144 (2008) 289–298.
[10] J.T. Richardson, B. Turk, M.V. Twigg, Appl. Catal. A: Gen. 148 (1996) 97–112.
[11] J.T. Richardson, M. Lei, B. Turk, K. Forster, M.V. Twigg, Appl. Catal. A: Gen. 110 (1994) 217–237.
[12] D.R. Goodman, Catalyst Handbook, in: M.V. Twigg (Ed.), Wolfe Publishing Ltd., London, 1996, pp. 161–174.
[13] J. Sehested, Catal. Today 111 (2006) 103–110.
[14] B. Valle, B. Aramburu, A. Remiro, J. Bilbao, A.G. Gayubo, Appl. Catal. B: Environ. 147 (2014) 402–410.
[15] J.T. Richardson, R. Scates, M.V. Twigg, Appl. Catal. A Gen. 246 (2003) 137–150.
[16] J.T. Richardson, R.M. Scates, M.V. Twigg, Appl. Catal. A Gen. 267 (2004) 35–46.
[17] J. Szekely, C.I. Lin, H.Y. Sohn, Chem. Eng. Sci. 28 (1973) 1975–1989.
[18] S.S.A. Syed-Hassan, C.Z. Li, Appl. Catal. A Gen. 398 (2011) 187–194.
[19] K.M. Ostyn, C.B. Carter, Surf. Sci. 121 (1982) 360–374.
[20] J.T. Richardson, B. Turk, M. Lei, K. Forster, M.V. Twigg, Appl. Catal. A Gen. 83 (1992) 87–101.
[21] Y. Iida, K. Shimada, Bull. Chem. Soc. Jpn. 33 (1960) 8–11.
[22] Y. Iida, K. Shimada, Bull. Chem. Soc. Jpn. 33 (1960) 1194–1196.
[23] W.J. Lee, C.-Z. Li, Appl. Catal. A Gen. 316 (2007) 90–99.
[24] G.W. Huber, S. Iborra, A. Corma, Chem. Rev. 106 (2006) 4044–4098.
[25] D. Wang, S. Czernik, D. Montane, M. Mann, E. Chornet, Ind. Eng. Chem. Res. 36 (1997) 1507–1518.
[26] X. Hu, G.X. Lu, Appl. Catal. B Environ. 88 (2009) 376–385.
[27] P. Pimenidou, G. Rickett, V. Dupont, M.V. Twigg, Bioresour. Technol. 101 (2010) 6389–6397.
[28] P. Pimenidou, G. Rickett, V. Dupont, M.V. Twigg, Bioresour. Technol. 101 (2010) 9279–9286.
[29] N. Giannakeas, A. Lea-Langton, V. Dupont, M.V. Twigg, Appl. Catal. B-Environ. 126 (2012) 249–257.
[30] A. Lea-Langton, R.M. Zin, V. Dupont, M.V. Twigg, Int. J. Hydrogen Energy 37 (2012) 2037–2043.
[31] L.B. McCusker, R.B. Von Dreele, D.E. Cox, D. Louer, P. Scardi, J. Appl. Crystallogr. 32 (1999) 36–50.
[32] M.S. Mettler, A.D. Paulsen, D.G. Vlachos, P.J. Dauenhauer, Green Chem. 14 (2012) 1284–1288.
[33] S.K. Sharma, F.J. Vastola, P.L. Walker, Carbon 35 (1997) 535–541.
[34] J. Barbier, Appl. Catal. 23 (1986) 225–243.
[35] A. Remiro, B. Valle, A.T. Aguayo, J. Bilbao, A.G. Gayubo, Fuel Process. Technol. 115 (2013) 222–232.
[36] M.M. Hossain, H.I. de Lasa, AIChE J. 53 (2007) 1817–1829.
[37] X. Hu, G. Lu, Green Chem. 11 (2009) 724–732.
[38] M. El-Guindy, W. Davenport, Metall. Trans. 1 (1970) 1729–1734.
[39] Y. Cao, B. Casenas, W.-P. Pan, Energy Fuels 20 (2006) 1845–1854.
[40] B. Jankovic, B. Adnadevic, S. Mentus, Chem. Eng. Sci. 63 (2008) 567–575.
[41] T.A. Utigard, M. Wu, G. Plascencia, T. Marin, Chem. Eng. Sci. 60 (2005) 2061–2068.
[42] M. Ishida, H.G. Jin, T. Okamoto, Energy Fuels 10 (1996) 958–963.
[43] Q. Zafar, A. Abad, T. Mattisson, B. Gevert, Energy Fuels 21 (2007) 610–618.
[44] F. Wang, X. Zeng, Y. Wang, H. Su, J. Yu, G. Xu, Fuel 164 (2016) 403–409.